Explicit Higher-Order FDTD Schemes for 3D Room Acoustic Simulation

Jelle van Mourik and Damian Murphy

***Abstract*—The Finite Difference Time Domain method is gaining popularity as a means to simulate and solve room acoustical problems. In this paper, a new set of stencils is defined that approximate the wave equation with a high degree of accuracy and lower dispersion error. Compared to the previously presented optimal scheme, the Interpolated Wideband scheme, our schemes are computationally less demanding and more practical to implement. They use at least 8 times less memory for the same audio rate and are an order of magnitude faster, although the former has a higher valid bandwidth. Despite their larger computational expense per node update, it is shown that our schemes on the whole use less memory and computation time than the Standard Rectilinear stencil, particularly when GPU implementations are employed. Lastly, a new way of visualizing and comparing valid bandwidth is recommended.**

***Index Terms*—Acoustics, finite difference time domain (FDTD), numerical methods, wave propagation.**

I. Introduction

OVER the last decade, the Finite Difference Time Domain (FDTD) method has become a commonly used algorithm in room acoustic modeling [1]–[4]. With computational power becoming more readily available, it is becoming an alternative to the faster geometric (or ray-based) modeling methods, such as ray tracing [5]–[7], beam tracing [8]–[10], and the radiosity method [11], [12]. As a wave-based approach, the FDTD method numerically solves the wave equation at a finite number of points in a discretised space. Because of this rigorous approach, wave effects such as diffraction and wave interference are inherently modelled, contrary to ray-based methods, in which these effects are not trivial to incorporate [13], [14]. Though conceptually different from the Digital Waveguide Mesh (DWM), it was shown that the FDTD is equivalent to a DWM approach when modelling wave propagation in the free field in 2 dimensions or more [15]–[17].

The FDTD algorithm has been described as an 'embarrassingly parallel' problem [18], referring to the idea that it is relatively trivial to perform the update phase of the algorithm in parallel rather than sequentially. General Purpose computation on Graphics Processing Units (GPGPU) provides a means to implement this algorithm in parallel. It has been shown that GPU implementations provide substantial performance gains, up to three orders of magnitude compared to equivalent CPU implementations [4], [19], [20]. However, the room impulse responses (RIRs) produced by the FDTD method suffer from dispersion error, rendering invalid the high and most of the mid-frequency part of the spectrum [3]. In a typical simulation at audio rate, only the lowest 10% of the bandwidth is considered valid, and dispersion error becomes perceptually noticeable around 12% to 15% of the sample rate [21]. Moreover, the FDTD method is very memory-intensive, and the requirements for simulations of typical rooms at audio-rate can easily exceed several gigabytes. Raghuvanshi *et al.* [22] devised an Adaptive Rectangular Decomposition (ARD) method which greatly reduces the computational requirements, although finite difference methods are still used at boundaries and at interconnecting decomposed rectangles. Moreover, they developed a system to auralise these precomputed results in real-time in a virtual environment [23].

Kowalczyk and Van Walstijn [3] presented a family of explicit second-order accurate stencils and analysed their dispersive properties and stability. They found that the Interpolated Wideband (IWB) scheme is the explicit update scheme that yields the most even dispersion pattern and is therefore preferred over the more commonly used Standard Rectilinear (SRL) scheme. Kowalczyk [24] also describes a Fourth Order Accurate (FOA) scheme as a special case of the second-order schemes, first described by [25], in which fourth-order error terms are cancelled out. However, despite showing a smaller dispersion error than the IWB scheme, it is an implicit scheme and therefore impractical to implement. A comprehensive overview of several FDTD implementations and the appropriate boundary conditions can found be in [26]. Fourth-order implicit schemes have also been studied by, for example, [25] and [27]. Hamilton and Bilbao [28], [29] investigated explicit fourth-order accurate schemes in two dimensions, and used numerical methods to find optimal update coefficients. To the best of the authors' knowledge, stencils of orders of accuracy higher than 4 have not been investigated in the framework of room acoustic modeling.

This paper investigates a family of higher-order accurate schemes called 'large-star stencils' [27]: schemes that only take nodes along the grid axes into their update equation. They offer improvements over the SRL but without the complex stencils required for other approaches, including IWB. The goal, therefore, is to identify an optimal scheme, better than SRL, that should be at least comparable to what is offered by IWB. The result will therefore be proposed for further study of the boundary problem, which will be subject to further

Manuscript received September 09, 2013; revised February 14, 2014; accepted June 22, 2014. Date of publication July 23, 2014; date of current version October 01, 2014. The associate editor coordinating the review of this manuscript and approving it for publication was Prof. Bozena Kostek.

The authors are with the Department of Electronics, University of York, York YO10 5DD, U.K. (e-mail: jvm502@york.ac.uk).

Color versions of one or more of the figures in this paper are available online at http://ieeexplore.ieee.org.

Digital Object Identifier 10.1109/TASLP.2014.2341913

work, possibly taking advantage of recent results relating to finite volume boundary solutions combined with FDTD [30], and leading to a general method to model spaces of arbitrary geometry.

These stencils have the advantage that they are particularly efficient and relatively easy to implement on a GPU device [31]. It will be shown that these stencils allow for large memory savings and consequently higher computational speed in our test cases. Moreover, compared to the commonly used SRL scheme, they provide a higher valid bandwidth and isotropy at low frequencies, combined with a significant memory saving. As the IWB scheme is considered the current state-of-art first order scheme, it is also included in our analysis. Compared to the IWB scheme, the higher-order stencils provide an even greater memory saving, but a smaller valid bandwidth. Lastly, a new way of graphing the quality of a stencil as a function of the maximum tolerated error is proposed.

The structure of the paper is as follows: Section II discusses the derivation, stability, and dispersive pattern of a second-order FDTD scheme. Section III extends this analysis to the family of large-star stencils and provides analytical and numerical data on dispersion and valid bandwidth thereof. In Section IV, the GPU implementation and test procedure to verify the model is described. Section V provides numerical and graphical results from the simulations. Conclusions are given in Section VI, including suggestions for future research.

II. Background

The starting point of the room acoustical model is the homogeneous acoustic wave equation:

$$\left(\frac{\partial^2}{\partial t^2} - c^2\nabla^2\right) p(\mathbf{x}, t) = 0, \tag{1}$$

where $p(\mathbf{x}, t)$ is the pressure at time t and position $\mathbf{x}$, c is the speed of sound, and the ∇^2 operator represents the second spatial derivative.

Considering the 1-dimensional case, and introducing the convenience notation $p_x^t \triangleq p(xX, tT)$, with spatial step (or grid spacing) X and time step $T = f_s^{-1}$, the second-order accurate discrete approximation of this equation is:

$$p_x^{t+1} - 2p_x^t + p_x^{t-1} \approx \lambda^2\left(p_{x-1}^t - 2p_x^t + p_{x+1}^t\right), \tag{2}$$

where $\lambda = \frac{cT}{X}$, commonly referred to as the Courant number. Solving this for p_x^{t+1} yields the well-known update equation for the 1-dimensional wave equation.

Von Neumann analysis can be employed to find this scheme's stability condition (see e.g. [32]). p_x^t can be substituted with a trial solution, which for future reference will be denoted as a linear operator $\mathcal{Q}$:

$$\mathcal{Q}\{p_x^t\} \triangleq e^{(\sigma+j\omega)T}e^{jk_xX} = z^T e^{jk_xX}, \tag{3}$$

where $z \triangleq e^{\sigma+j\omega}$, j is the imaginary unit $j^2 = -1$, and $\sigma, \omega \in \mathbb{R}$. This is essentially a single term from the Z-transform over time and discrete Fourier transform over space of p_x^t. As both are linear transformations, it suffices to prove stability for only one term. In order for the scheme to be stable, $-1 \leq \Re(z) \leq 1$ must hold for all ω, from which follows that $\sigma \leq 0$.

Testing our trial solution is equivalent to applying the $\mathcal{Q}$ operator on both sides in (2), and after using common goniometric identities results in:

$$z^2 + (A-2)z + 1 = 0, \tag{4}$$

where $A = 4\lambda^2\sin^2(\frac{k_xX}{2})$. Solving this equation for z and inserting it into the stability condition for z results into the stability bound on A:

$$0 \leq A \leq 4, \tag{5}$$

which leads to the Courant stability condition [33]:

$$\lambda^2\sin^2\left(\frac{k_xX}{2}\right) \leq 1 \quad \forall X, k_x \in \mathbb{R} \quad \Rightarrow \quad \lambda \leq 1. \tag{6}$$

The dispersive properties of the 1D FDTD scheme can be analyzed by finding the angular phase velocity ω_ϕ of the traveling wave. Assuming harmonic waves ($\sigma = 0$) and writing $\omega_\phi = \omega$, we arrive at an expression for the angular phase velocity:

$$-4\sin^2\left(\frac{\omega_\phi T}{2}\right) = -4\lambda^2\sin^2\left(\frac{k_xX}{2}\right) \tag{7}$$

$$\omega_\phi = \frac{2}{T}\arcsin\left(\pm\lambda\sin\left(\frac{k_xX}{2}\right)\right). \tag{8}$$

At the Courant stability limit $\lambda = 1$, the phase velocity becomes $v_\phi = \frac{\omega_\phi}{k_x} = \frac{X}{T} = c$. In other words, at the stability limit, the 1D FDTD stencil is dispersionless at all frequencies. For lower values of λ, the phase velocity is not constant, which will result in a mistuning of higher harmonics.

In three dimensions, the approach is largely the same and can be found in, for example, [3], [34, p. 311]. Writing $F(k_x, k_y, k_z) = \sin(\frac{k_xX}{2}) + \sin(\frac{k_yX}{2}) + \sin(\frac{k_zX}{2})$, we can arrive at the stability condition (5) where now:

$$A = 4\lambda^2 F(k_x, k_y, k_z), \tag{9}$$

with $k_{x,y,z}$ being the wave numbers along the Cartesian axes. From this, it can be deduced that the Courant stability condition in three dimensions is $\lambda \leq \frac{1}{3}\sqrt{3}$. The dispersion analysis is less trivial, since the propagation direction now plays a role too. The angular phase velocity now becomes:

$$\omega_\phi = \frac{2}{T}\arcsin\left(\pm\lambda\sqrt{F(k_x, k_y, k_z)}\right), \tag{10}$$

where in 3 dimensions:

$$v_\phi = \frac{\omega_\phi}{\sqrt{k_x^2 + k_y^2 + k_z^2}}. \tag{11}$$

This can be interpreted as the wave speed along any direction as determined by $k_{x,y,z}$, which in an ideal situation should equal c for all possible combinations of axial wave numbers. However, it can be verified that only along the diagonal, when $k_x = k_y = k_z$, the system is dispersionless. The highest dispersion can be observed along a grid axis, e.g. when $k_y = k_z = 0$.

A more general difference approximation, of which the SRL scheme is part, has been presented in [3]. In these schemes, the differences along the diagonal axes are also taken into account to give a more accurate estimation, at the cost of more calculations. The study also gives the update equations, stability limits, and dispersive properties of all of these stencils. Most notably, the IWB scheme seems to give the lowest dispersion and the highest isotropy of all, and is therefore commonly considered the state-of-art second-order finite difference scheme (in both 2D and 3D). For this reason, this scheme has been included in every analysis in this paper as a benchmark. The stability condition for the IWB scheme in 3D is $\lambda \leq 1$; its dispersive properties are stated in [3, Eq. (24)].

For a measure of the quality of a stencil, Kowalczyk and Van Walstijn [3] proposed to use the fraction of the bandwidth that can be modelled without exceeding a predefined accuracy error ϵ. They used several values in their analysis: $\epsilon = 2\%, 4\%, 8\%$. Savioja [21] used a more tolerant criterion of $\epsilon = 10\%$, and Hamilton and Bilbao [29] used $\epsilon = 1\%$ for 2D stencils. In an attempt to find a perceptually meaningful value of ϵ, Southern [21] conducted a study after the limits as of which dispersion becomes noticeable. He found that in an SRL scheme sampled at $f_s = 5000$ Hz, dispersion becomes perceptually noticeable around 0.12 to 0.15 f_s. This corresponds to an ϵ between 5% and 8%.

Hamilton and Bilbao [29] performed an extensive research on fourth-order accurate schemes in two dimensions. Using a linear combination of difference approximations over the axes and diagonals of a rectangular grid, they investigated the dispersive and isotropic properties of several different possibilities. They used numeric optimisation techniques to find the coefficients that minimise the wave speed error up to some given frequency. However, extending their approach to three dimensions and/or orders higher than 4 would be impractical, as the large number of neighboring nodes required for an update equation would become a bottleneck for the implementation. Large-star stencils offer an alternative, as the number of required nodes in three dimensions is $6n + 1$, instead of $(n + 1)^3$ for more general methods, where n represents the order of accuracy of the stencil.

III. Derivation of Higher-Order Stencils

In order to generalize the approach outlined in the previous section to higher-order stencils, a better approximation to the second derivative has to be found. First of all, it is important to decide which derivative(s) in (1) to approximate with higher-order coefficients. We choose to keep the second-order approximation for the second derivative over time, as to not increase the memory requirements of the FDTD algorithm. The second derivative with respect to space on the contrary will be approximated with a higher-order scheme. This will result in a higher computational load per node update, but the memory requirements will not increase. In the following paragraph, we use Lagrangian interpolation to find the update coefficients for a fourth-order scheme. Alternative derivation can be found in, for example, [35], [36].

Let $g(x)$ be a Lagrange polynomial, i.e. the polynomial of least degree, that passes through the points $(0, f_0), (X, f_1), \ldots, (4X, f_4)$. $g(x)$ must therefore be of degree four:

$$g(x) = a_0 + a_1 x + a_2 x^2 + a_3 x^3 + a_4 x^4. \tag{13}$$

As the polynomial passes through all 5 points, the following must hold:

$$\begin{pmatrix} 0 & 0 & 0 & 0 & 1 \\ X^4 & X^3 & X^2 & X & 1 \\ 16X^4 & 8X^3 & 4X^2 & 2X & 1 \\ 81X^4 & 27X^3 & 9X^2 & 3X & 1 \\ 256X^4 & 64X^3 & 16X^2 & 4X & 1 \end{pmatrix} \begin{pmatrix} a_4 \\ a_3 \\ a_2 \\ a_1 \\ a_0 \end{pmatrix} = \begin{pmatrix} f_0 \\ f_1 \\ f_2 \\ f_3 \\ f_4 \end{pmatrix}. \tag{14}$$

As this is a system of 5 equations with 5 unknowns, the polynomial coefficients, there is exactly one solution to this system, which can be found efficiently by using the inverse matrix method to obtain:

$$\begin{cases} a_0 = f_0 \\ a_1 = \frac{-25f_0+48f_1-36f_2+16f_3-3f_4}{12X} \\ a_2 = \frac{35f_0-104f_1+114f_2-56f_3+11f_4}{24X^2} \\ a_3 = \frac{-5f_0+18f_1-24f_2+14f_3-3f_4}{12X^3} \\ a_4 = \frac{f_0-4f_1+6f_2-4f_3+f_4}{24X^4}. \end{cases} \tag{15}$$

In order to find the update coefficients for a centred difference scheme, this scheme can be evaluated in the middle, i.e. at $2X$,

$$\begin{aligned} 0 &\leq -\lambda^2 \left| \mathcal{Q} \left\{ -\frac{1}{12} p_{x-2} + \frac{4}{3} p_{x-1} - \frac{5}{2} p_x + \frac{4}{3} p_{x+1} - \frac{1}{12} p_{x+2} \right\} z^{-T} e^{-jkX} \right| \leq 4 \\ 0 &\leq -\lambda^2 \left| \left(-\frac{1}{12} \left(e^{-2jkX} - 2 + e^{2jkX} \right) z^T e^{jkX} + \frac{4}{3} \left(e^{-jkX} - 2 + e^{jkX} \right) z^T e^{jkX} \right) z^{-T} e^{-jkX} \right| \leq 4 \\ 0 &\leq \lambda^2 \underbrace{\left| \frac{4}{3} \sin^2 \left(\frac{kX}{2} \right) - \frac{1}{12} \sin^2 (kX) \right|}_{\text{maximum value: } \frac{4}{3}} \leq 1 \\ 0 &\leq \lambda \leq \sqrt{\frac{3}{4}} \end{aligned} \tag{12}$$

TABLE I
THE UPDATE COEFFICIENTS FOR A CENTRED DIFFERENCE APPROXIMATION UP TO THE SIXTEENTH ORDER OF ACCURACY. THE STABILITY LIMIT $\lambda_{\max}$ IS THAT OF THE 1-DIMENSIONAL STENCIL. THE MEMORY SAVING REPRESENTS THE THEORETICAL MAXIMUM MEMORY SAVING FOR A STENCIL WITH RESPECT TO THE SECOND-ORDER STENCIL

	p_{x-8}	p_{x-7}	p_{x-6}	p_{x-5}	p_{x-4}	p_{x-3}	p_{x-2}	p_{x-1}	p_x	p_{x+1}	p_{x+2}	p_{x+3}	p_{x+4}	p_{x+5}	p_{x+6}	p_{x+7}	p_{x+8}	$\lambda_{\max,1D}$	Memory saving 3D
2^{nd}	0	0	0	0	0	0	0	$\frac{1}{2}$	-1	$\frac{1}{2}$	0	0	0	0	0	0	0	1	0%
4^{th}	0	0	0	0	0	0	$-\frac{1}{12}$	$\frac{4}{3}$	$-\frac{5}{2}$	$\frac{4}{3}$	$-\frac{1}{12}$	0	0	0	0	0	0	$\sqrt{\frac{3}{4}}$	35.1%
6^{th}	0	0	0	0	0	$\frac{1}{90}$	$-\frac{3}{20}$	$\frac{3}{2}$	$-\frac{49}{18}$	$\frac{3}{2}$	$-\frac{3}{20}$	$\frac{1}{90}$	0	0	0	0	0	$\sqrt{\frac{45}{68}}$	46.2%
8^{th}	0	0	0	0	$-\frac{1}{560}$	$\frac{8}{315}$	$-\frac{1}{5}$	$\frac{8}{5}$	$-\frac{205}{72}$	$\frac{8}{5}$	$-\frac{1}{5}$	$\frac{8}{315}$	$-\frac{1}{560}$	0	0	0	0	$\sqrt{\frac{315}{512}}$	51.7%
10^{th}	0	0	0	$\frac{1}{3150}$	$-\frac{5}{1008}$	$\frac{5}{126}$	$-\frac{5}{21}$	$\frac{5}{3}$	$-\frac{5269}{1800}$	$\frac{5}{3}$	$-\frac{5}{21}$	$\frac{5}{126}$	$-\frac{5}{1008}$	$\frac{1}{3150}$	0	0	0	$\sqrt{\frac{75}{128}}$	55.2%
12^{th}	0	0	$-\frac{1}{16632}$	$\frac{2}{1925}$	$-\frac{1}{112}$	$\frac{10}{189}$	$-\frac{15}{56}$	$\frac{12}{7}$	$-\frac{5369}{1800}$	$\frac{12}{7}$	$-\frac{15}{56}$	$\frac{10}{189}$	$-\frac{1}{112}$	$\frac{2}{1925}$	$-\frac{1}{16632}$	0	0	$\sqrt{\frac{51975}{91904}}$	57.5%
14^{th}	0	$\frac{1}{84084}$	$-\frac{7}{30888}$	$\frac{7}{3300}$	$-\frac{7}{528}$	$\frac{7}{108}$	$-\frac{7}{24}$	$\frac{7}{4}$	$-\frac{266681}{88200}$	$\frac{7}{4}$	$-\frac{7}{24}$	$\frac{7}{108}$	$-\frac{7}{528}$	$\frac{7}{3300}$	$-\frac{7}{30888}$	$\frac{1}{84084}$	0	$\sqrt{\frac{4729725}{8593664}}$	59.2%
16^{th}	$-\frac{1}{411840}$	$\frac{16}{315315}$	$-\frac{2}{3861}$	$\frac{112}{32175}$	$-\frac{7}{396}$	$\frac{112}{1485}$	$-\frac{14}{45}$	$\frac{16}{9}$	$-\frac{1077749}{352800}$	$\frac{16}{9}$	$-\frac{14}{45}$	$\frac{112}{1485}$	$-\frac{7}{396}$	$\frac{112}{32175}$	$-\frac{2}{3861}$	$\frac{16}{315315}$	$-\frac{1}{411840}$	$\sqrt{\frac{4729725}{8781824}}$	60.5%

and differentiated twice to find the approximation of the second derivative:

$$g''(2X) = \frac{-f_0 + 16f_1 - 30f_2 + 16f_3 - f_4}{12X^2}, \tag{16}$$

which immediately gives the fourth-order accurate update stencil of a second derivative: $\{-\frac{1}{12}, \frac{4}{3}, -\frac{5}{2}, \frac{4}{3}, -\frac{1}{12}\}$.

Centred difference schemes only exist when the stencil has a single middle point, so this approach can be generalised to stencils of nth order, where n is an even positive integer. One will always arrive at a determinate system of $n+1$ equations with $n+1$ unknowns, which can be solved and evaluated at the centre point. Table I presents all the update coefficients up to sixteenth order.

A. Stability Analysis

Due to the extra coefficients that come into play in large-star systems, the wave cannot be broken down into a single sine wave. Instead, (4) in the general case becomes:

$$z - 2 + z^{-1} = \lambda^2 \mathcal{Q}\left\{\nabla^2 p_x^t\right\} z^{-T} e^{-jk_x X}, \tag{17}$$

where ∇^2 may be approximated by a centred-difference scheme of arbitrary order. Analogous to (5), a bound on the right-hand side of this equation can be derived that guarantees stability:

$$0 \leq -\lambda^2 \left|\mathcal{Q}\left\{\nabla^2 p\right\} z^{-T} e^{-jk_x X}\right| \leq 4. \tag{18}$$

To illustrate this, the stability condition for the fourth-order 1D stencil is derived in (12). λ is then bound by $0 \leq \lambda \leq \sqrt{\frac{3}{4}}$. A similar analysis can be performed on all stencils to find a stability condition for each. Table I also presents the stability limit for λ up to sixteenth order for a 1-dimensional stencil. It can easily be verified that for an N-dimensional stencil, the stability limit follows as:

$$\lambda_{\max,N} = \frac{\lambda_{\max,1D}}{\sqrt{N}}. \tag{19}$$

Taking a closer look at the stencil coefficients, it can be observed that a numerical bound seems in place: the stability bound on λ^2 seems to converge to approximately $\frac{1}{2}$. This is related to the fact that the dominant term is given by the direct neighbor nodes ($p_{x\pm1}$), and these coefficients follow the pattern $\frac{n}{\frac{n}{2}+1}$ for all but the second-order case. This fraction converges to $\frac{1}{2}$ in the limit of $n \to \infty$. The true convergence is lower, however, due to the contribution of the higher order coefficients. Finding a full analytical proof for a value of convergence is an open problem, though, and will be subject of further work and testing.

If we assume that the speed of sound and the sample rate of the simulations remain the same, a change in the Courant number implies a change in the grid spacing. For every increase in order of accuracy, the grid spacing has to go up. In terms of simulating the space, this means that a smaller number of grid points is required to simulate the same space. As this paper is mostly concerned with 3D simulations, we will consider the memory savings of an nth order scheme in 3 dimensions with respect to the 3D SRL scheme:

$$\begin{aligned}\text{Relative memory usage} &= \left(\frac{\lambda_{n,3D}}{\lambda_{2^{\text{nd}},3D}}\right)^3 = \left(\frac{\lambda_{n,3D}}{\sqrt{\frac{1}{3}}}\right)^3 \\ &= \lambda_{n,1D}^3. \end{aligned} \tag{20}$$

In Table I, the memory savings (in percentages) are listed for all schemes up to sixteenth order. As $\lambda_{\max}$ converges to approximately $\frac{1}{\sqrt{2}}$ for orders of accuracy within the scope of practical implementation, the theoretical maximum on memory saving using this method is 64.6%.

The stability limit of the 3D IWB scheme is $\lambda_{\text{IWB,3D}} = 1$. Compared to the SRL scheme, it therefore uses $3^{\frac{3}{2}} \approx 5.19$ times as much memory for the same simulation. Compared to the fourth order scheme, this is even 8 times.

B. Dispersion Analysis

The dispersion patterns of higher-order stencils are no longer trivial even for the 1-dimensional case. They can again be obtained by taking the Fourier transform of the spatial stencil, in the same way as in (10). For the fourth-order stencils, the angular wave speed is given by:

$$\omega_\phi = \frac{2}{T}\arcsin\left(\pm\lambda\left[\frac{4}{3}F(k_x,k_y,k_z) - \frac{1}{12}F(k_x,k_y,k_z)\right]^{\frac{1}{2}}\right) \tag{21}$$

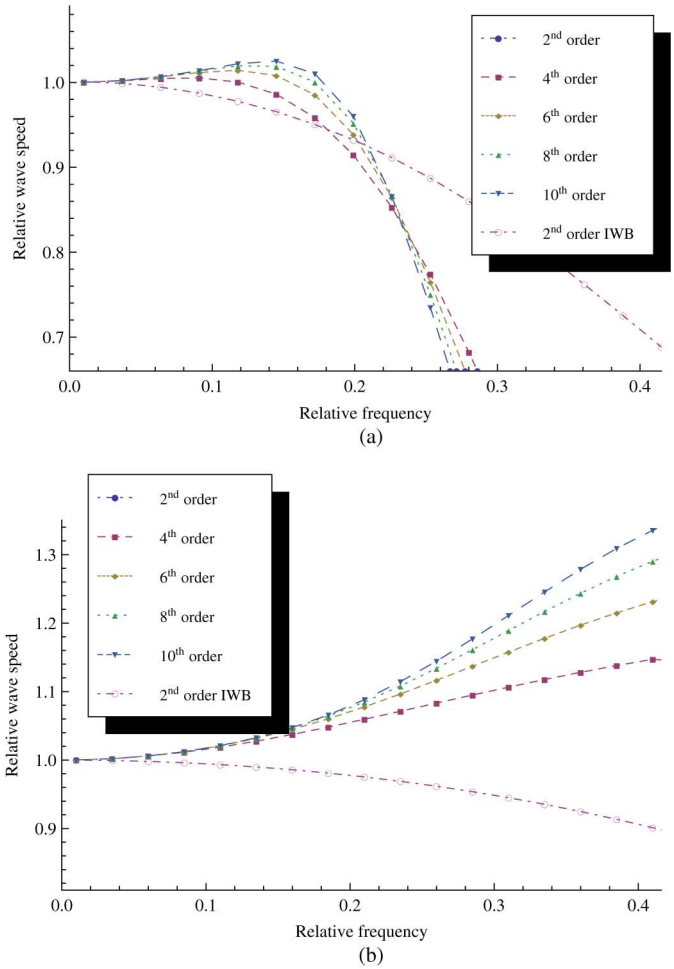

Fig. 1. (a) and (b) show the relative phase velocity $\frac{v_\phi}{c}$ along a grid axis and diagonal, respectively, for 0 up to 0.4 f_s.

Also for higher-order schemes, dispersion is minimised by evaluating it at its Courant stability limit. However, the highest dispersion can no longer only be found along the axes of the grid, but also along the diagonals. A convenient way of visualising a comparison is therefore to plot the dispersion patterns of each at their respective stability limit. Fig. 1 shows the relative wave speed along the grid axis and diagonal for stencils of second- to tenth-order of accuracy. Along the grid axis, the general tendency is that the wave velocity remains relatively stable for slightly longer than in the second-order case. It rises slightly (more so for stencils of higher order) and then drops around $0.2 f_s$. In contrast, the IWB stencil shows a smooth roll-off that decays slower, although it is slightly less accurate for low frequencies.

On the contrary, along the diagonal the wave velocity becomes increasingly overestimated with the frequency increasing, more so for stencils of higher order. The stencils with order of accuracy higher than 10 follow a similar trend, but have been omitted from the plot for the sake of clarity. The difference with the IWB scheme is apparent, as this shows a smoother and slower roll-off (downwards instead of up) than all the higher-order stencils.

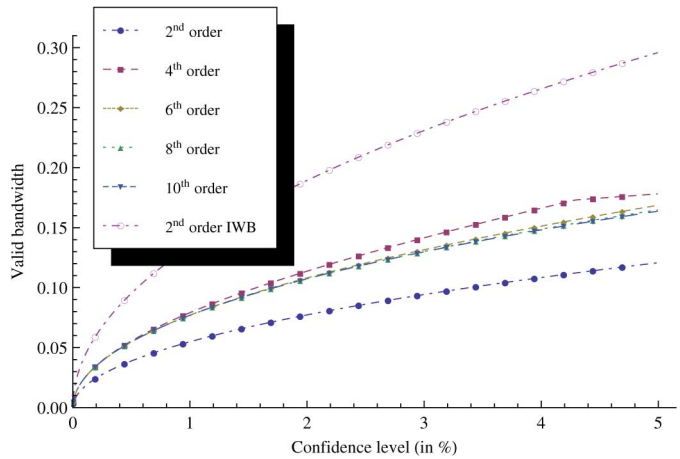

Fig. 2. The maximum allowed isotropy error ϵ (in percentages) versus the valid bandwidth for the second up to tenth-order stencil.

TABLE II
THE MINIMUM REQUIRED ARITHMETIC OPERATIONS FOR A SINGLE NODE UPDATE PER STENCIL

Stencil	Add/Substract	Multiply	Memory access
2nd order	6	1	7
4th order	13	3	13
6th order	19	4	19
8th order	25	5	25
10th order	31	6	31
IWB	27	4	27

As the highest dispersion cannot solely be observed along one axis, the quality of the stencils is difficult to compare by means of dispersion plots. As a way to visualize the relative quality of different stencils, we propose to use a plot of the maximum allowed accuracy error ϵ versus the corresponding valid bandwidth. Such a plot makes it possible to see exactly how much of the bandwidth can be considered valid for a given accuracy error margin ϵ.

Fig. 2 shows such a plot for the second up to tenth-order stencil. It is clear from the plot that the second-order SRL scheme performs worst of all, with only a 7.7% valid bandwidth at a 2% error interval. Remarkably, of all higher-order stencils, the fourth-order accurate scheme provides the highest valid bandwidth for all ϵ. This is due to the fact that the dispersion along the diagonal is now the main limiting factor, and the fourth-order scheme shows the least dispersion in this direction, save for the dispersionless second-order stencil. The IWB scheme gives a significantly better performance than all large-star systems. It can therefore be concluded that in terms of dispersion, the fourth-order accurate scheme is the best among the analyzed higher-order schemes, approximately 1.5 times better than the SRL scheme. After that, the quality deteriorates with each increase in order, although the differences are marginal and negligible for orders of accuracy higher than 10. The IWB scheme is approximately 1.65 times more accurate than the fourth order accurate scheme, although this comes at the price of an eightfold increase in memory usage.

TABLE III
THE COMPUTATIONAL SPEED OF THE THREE DIFFERENT SCENARIOS FOR STENCILS OF SECOND UP TO SIXTEENTH ORDER, AND THE SECOND-ORDER IWB SCHEME. THE ROOM DIMENSIONS ARE GIVEN IN NUMBER OF NODES, THE COMPUTATIONAL SPEED IN FRAMES PER SECOND

	Small room ($1.5 \times 1.25 \times 1.0$)			Medium-sized room ($5.0 \times 3.5 \times 2.0$)			Large room ($7.0 \times 5.0 \times 4.0$)		
Order	Dimensions	# nodes	fps	Dimensions	# nodes	fps	Dimensions	# nodes	fps
2^{nd}	$111 \times 92 \times 74$	755 688	3967.0	$370 \times 259 \times 148$	14 182 840	295.3	$519 \times 370 \times 296$	56 840 880	73.3
4^{th}	$96 \times 80 \times 64$	491 520	5750.4	$321 \times 224 \times 128$	9 203 712	402.4	$449 \times 321 \times 256$	36 897 024	99.3
6^{th}	$90 \times 75 \times 60$	405 000	5365.6	$301 \times 211 \times 120$	7 621 320	412.3	$422 \times 301 \times 241$	30 612 302	107.7
8^{th}	$87 \times 72 \times 58$	363 312	4944.3	$290 \times 203 \times 116$	6 828 920	422.4	$407 \times 290 \times 232$	27 382 960	105.0
10^{th}	$85 \times 70 \times 56$	333 200	4565.5	$283 \times 198 \times 113$	6 331 842	372.6	$397 \times 283 \times 227$	25 503 677	98.8
12^{th}	$83 \times 69 \times 55$	314 985	4260.3	$278 \times 195 \times 111$	6 017 310	353.2	$390 \times 278 \times 223$	24 177 660	95.3
14^{th}	$82 \times 68 \times 55$	306 680	4150.1	$275 \times 192 \times 110$	5 808 000	351.1	$385 \times 275 \times 220$	23 292 500	90.8
16^{th}	$81 \times 68 \times 54$	297 432	4340.9	$272 \times 190 \times 108$	5 581 440	416.7	$381 \times 272 \times 217$	22 488 144	102.4
2^{nd}IWB	$192 \times 160 \times 128$	3 932 160	310.1	$642 \times 449 \times 256$	73 794 048	18.7	$899 \times 642 \times 513$	296 082 054	[overflow]

IV. A GPU IMPLEMENTATION OF THE HIGHER-ORDER FDTD METHOD

GPU implementations of the FDTD algorithm have brought the method within the scope of practical use due to the large performance gain [4], [20]. It is therefore worthwhile to discuss the implementations of higher-order stencils in this scope. A significant amount of work has been done in the area of parallelising the FDTD method. Most notably [20], [31], [37] discussed the details of GPU implementations using Nvidia's Compute Unified Device Architecture (CUDA). In this paper, the implementation by Micikevicius [31] is closely followed, as it is easily extensible and has been designed to deal with spatial stencils of a higher order. Moreover, it aims at minimising read-redundancy by transferring blocks of nearby nodes' pressure values to shared memory, after which data can be accessed more efficiently. This is particularly useful for higher-order stencils, which require many memory reads per node update. As implementations may very across devices and architectures, Table II shows the minimum number of arithmetic operation that is required for a single node update.

The code was extended to suit a stencil of order $n \leq 16$. Texture memory was used to store the pressure values in order to allow more efficient memory access. The update coefficients were placed on the GPU's constant memory. Experiments were performed on a GPU device with Kepler architecture, compute capability 3.0, and a clock rate of 980 MHz. It was found that block dimensions of 16×16 threads provided the optimal performance.

As Micikevicius' algorithm can only be applied to stencils that use on-axis neighboring points (i.e. large-star stencils), a new algorithm had to be developed to implement the IWB in CUDA. In order to be able to make a fair comparison, an adaptation of said algorithm was therefore developed. Our algorithm also tries to minimise read-redundancy, which would be particularly prevalent in the IWB scheme, as it requires 27 memory accesses per node update. As in Micikevicius' algorithm, the blocks cover the entire xy-plane, and iteration per thread takes place over the z-axis. The shared memory is a circular buffer that contains 3 instead of one slice, however, for $p_{x,y,z-1}$, $p_{x,y,z}$, $p_{x,y,z+1}$. This shared memory buffer is updated from the device memory at each iteration over the z-axis, after which each node updates its value with the values from shared memory. In order to maximize the performance, only the value of the node at the receiver position was transferred from GPU to CPU at each time step.

V. RESULTS

A. Test Set-Up

Three scenarios were defined, all shoebox type rooms of unequal dimension, one large ($7.0 \times 5.0 \times 4.0$), one medium-sized ($5.0 \times 3.5 \times 2.0$), one small ($1.5 \times 1.25 \times 1.0$). All simulations were run at an audio rate of 44100 kHz, at the respective stability limit of each stencil. From this, the grid spacing and thus the number of nodes in the simulation was calculated. The boundaries were all clamped at 0, i.e. phase-reversing perfectly reflective boundaries. The grid excitation was a Dirac impulse implemented as a soft/transparent source [38]. A raw impulse response was generated by taking the value of a grid point at each time step at a fixed receiver position. Post-processing and convolution with anechoic material would be necessary to auralize the acquired impulse responses. This is beyond the scope of this paper, however, and has been extensively studied by, for example, [39]–[41].

B. Performance Speed

The computation speed of the simulations are presented in Table III. The dimensions (in number of nodes), number of nodes, and frames per second (fps) have been listed for all cases. It is immediately clear that the second-order scheme is not optimal: it uses too many nodes, which is a bottleneck for the performance. The fourth- and sixth-order schemes perform significantly better: they are around 40% faster and use less memory. In the medium-sized room, the eighth-order stencil has the best overall performance, although this is not the case in the other two scenarios. For orders of accuracy 8 up to 14, the computational speed decreases with every increase in order. This can be explained by the fact that the relative memory gain is smaller for each increase in order, and is outweighed by the increasing computational requirements.

Interestingly, the sixteenth order stencil shows a sudden increase in performance again. In the medium-sized room, it even matches the sixth-order stencil in speed. This can most likely be attributed to more efficient memory accessing due to memory coalescing on the GPU device.

Because of the large amount of memory required by the IWB scheme at the same audio rate, it performs fairly poorly

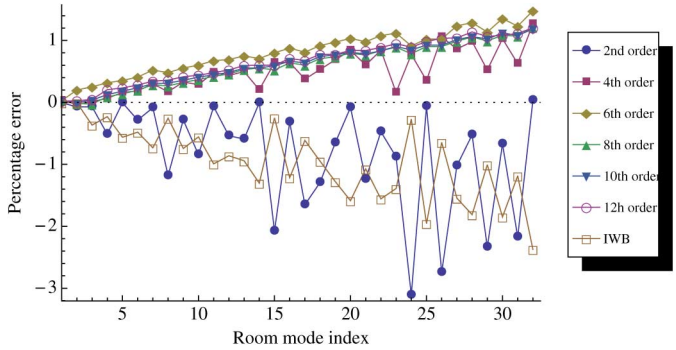

Fig. 3. The percentage error of each measured room mode with respect to its theoretical value, for each mode index i. The mode indices are ordered, and their axial configuration can be found in Table IV.

compared to the large-star stencils. As mentioned before, the memory requirement is 5.19 times that of the SRL scheme, and 13.14 times that of the sixteenth order scheme. Also, the number of arithmetic operations per node update is high and more demanding for the GPU because of the many memory access requests. As a result, the performance speed in the three test cases is more than an order of magnitude slower. In the large room, the room could not be modelled with this method because of a memory overflow.

It is important to note that the valid bandwidth that results from an IWB analysis is significantly higher than that of the higher-order stencils (see Fig. 2). Modelling the same room at a lower sample rate and upsampling to the same audio rate will therefore yield more favourable results. However, even when applying this technique, the performance does not exceed the fourth-order scheme: the IWB scheme's valid bandwidth is approximately 1.65 times higher than the fourth-order accurate stencil, so the memory usage could be reduced $1.65^3 \approx 4.49$ times. This is still larger than the memory requirements of the fourth-order scheme, and requires the inherently slower algorithm.

C. Spectral Analysis

In order to verify the results of the different FDTD schemes, another scenario was defined: a cube of $16 \times 16 \times 16$ nodes. The cubical shape was chosen because the room modes across all axes should be equal. The small room size makes it possible to make dispersion error visible in the frequency spectrum. Impulse responses of 10 s were obtained by running the same scenario for all stencils at audio rate at their respective stability limit. Hence, the physical size of the room varies, and the room modes were computed accordingly for each stencil. The source and receiver were positioned in opposite corners as to accommodate excitation of as many different room modes as possible. The boundaries were again perfectly reflective phase reversing surfaces.

Fig. 4 shows the frequency spectra up to $0.1 f_s$, with the theoretical room modes as dotted lines. It can be clearly observed that all stencils show some frequency warping higher up in the spectrum. The second-order schemes are the only ones that show a frequency drift to the left, which becomes visible around the fourth peak in the spectrum. In the other stencils, the room modes become increasingly higher than the theoretical

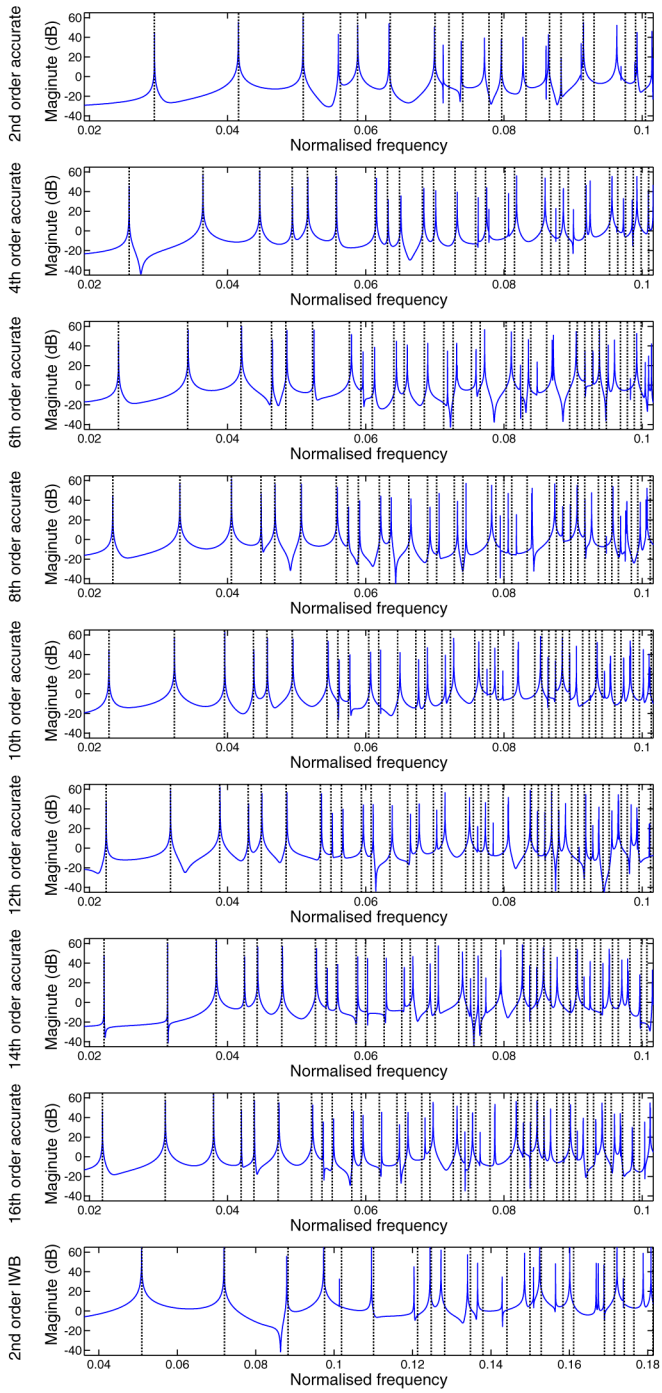

Fig. 4. The frequency spectrum (from 0.02 up to $0.1 f_s$) of the impulse responses of a cubical $16 \times 16 \times 16$ room. The dotted lines show the theoretical room modes for each case. Note that the results from the IWB scheme are shown on a different scale, as the room modes only show much higher in the normalised spectrum.

mode values. This is in accordance with the dispersion analysis presented in Section III-B: using higher-order stencils results in an overestimated wave speed for the majority of directions.

In order to compare and objectively quantify the modal shifts, a table was constructed with the measured peaks versus their theoretical values. The theoretical room modes were calculated for each model separately and matched to the peak values observed in Fig. 4, and the percentage error for each measured peak was computed. Fig. 3 plots the percentage error for each

TABLE IV
THE INDEX OF THE ROOM MODE (AS ALSO USED IN FIG. 3) VERSUS ITS AXIAL CONFIGURATIONS $\{x, y, z\}$. AS THE TEST CASE WAS A CUBE, ALL PERMUTATIONS OF THE SAME AXIAL CONFIGURATIONS ARE EQUAL, SO ONLY ONE OF EACH IS LISTED

$1 \rightarrow \{ 1, 1, 1 \}$	$12 \rightarrow \{ 2, 2, 4 \}$	$23 \rightarrow \{ 2, 3, 5 \}$
$2 \rightarrow \{ 1, 1, 2 \}$	$13 \rightarrow \{ 1, 3, 4 \}$	$24 \rightarrow \{ 1, 1, 6 \}$
$3 \rightarrow \{ 1, 2, 2 \}$	$14 \rightarrow \{ 3, 3, 3 \}$	$25 \rightarrow \{ 3, 4, 4 \}$
$4 \rightarrow \{ 1, 1, 3 \}$	$15 \rightarrow \{ 1, 1, 5 \}$	$26 \rightarrow \{ 1, 2, 6 \}$
$5 \rightarrow \{ 2, 2, 2 \}$	$16 \rightarrow \{ 2, 3, 4 \}$	$27 \rightarrow \{ 1, 4, 5 \}$
$6 \rightarrow \{ 1, 2, 3 \}$	$17 \rightarrow \{ 1, 2, 5 \}$	$28 \rightarrow \{ 3, 3, 5 \}$
$7 \rightarrow \{ 2, 2, 3 \}$	$18 \rightarrow \{ 2, 2, 5 \}$	$29 \rightarrow \{ 2, 2, 6 \}$
$8 \rightarrow \{ 1, 1, 4 \}$	$19 \rightarrow \{ 1, 4, 4 \}$	$30 \rightarrow \{ 2, 4, 5 \}$
$9 \rightarrow \{ 1, 3, 3 \}$	$20 \rightarrow \{ 3, 3, 4 \}$	$31 \rightarrow \{ 2, 3, 6 \}$
$10 \rightarrow \{ 1, 2, 4 \}$	$21 \rightarrow \{ 1, 3, 5 \}$	$32 \rightarrow \{ 4, 4, 4 \}$
$11 \rightarrow \{ 2, 3, 3 \}$	$22 \rightarrow \{ 2, 4, 4 \}$	

of the first 32 room modes. The room modes are indexed according to their theoretical occurrence order, and the exact configurations are shown in Table IV. As all room dimensions were equal, permutations of axial configurations were ignored.

The results presented in Fig. 3 are in close agreement with the theoretical results in dispersion predicted in Section III-B. The two second-order schemes only show a negative dispersion, and both show distinctive differences in wave speed for different modes. It can be noted that for the SRL's modal series where one axial direction dominates over any other (e.g. {1, 1, 3}, {1, 1,4}), the error is greater than with other modes due to the fact that dispersion is maximal for directions aligned axially with the FDTD grid. For the IWB's modal series, the reverse is true, which is indeed predicted by theoretical dispersion analysis [3]. Modes higher up in the spectrum are often rearranged as a result of this effect. The higher-order stencils show a smoother dispersion pattern and model an increased wave speed. As predicted in Fig. 2, the fourth-order stencil shows the least dispersion, though its dispersion pattern is evidently less smooth than the stencils of higher orders. With the order of the stencil increasing the stencils become more isotropic and the dispersion pattern for low frequencies becomes more even across all directions. There is therefore potential to apply frequency warping techniques [42] to improve the accuracy further, but this is beyond the scope of this paper.

VI. CONCLUSION AND DISCUSSION

The update coefficients for higher-order FDTD stencils have been derived using the well-known Lagrange polynomial approximation method. Analytical expressions for the dispersion patterns have been derived, and it was shown that higher-order stencils are less dispersive at low frequencies, thereby providing a higher valid bandwidth. Of the higher-order stencils, the fourth-order scheme was shown to be optimal in terms of valid bandwidth for all accuracy errors $\epsilon < 5\%$. The current state-of-art stencil, the IWB, is approximately 1.65 times more accurate than the fourth-order scheme over the same range.

It was shown that GPU implementations of said algorithm benefit greatly from higher-order stencil implementations. As the stability limit for the Courant number drops with each increase in order, the grid spacing has to go up, assuming the sample rate and speed of sound remain constant. As a result, the higher-order stencils save on memory and computation time, all of them outperforming the second-order scheme. The fourth and sixth come out as the fastest, as they combine a high relative memory saving with a relatively low computational load. The memory requirements of the IWB are 8 times higher than the fourth-order accurate scheme, and is impractical to implement due to the large number of memory accesses required. As a result, despite its higher valid bandwidth, it is greatly outperformed by higher-order stencils. The frequency spectra of impulse responses were analysed and confirm that higher-order stencils produce a valid outcome, with more evenly distributed error across low frequencies than the SRL scheme.

It has been shown that employing higher-order stencils provides computational and memory benefits. However, it introduces new questions regarding the treatment of boundaries, as the locally reacting surfaces approach in [24] cannot be used without adaptation. The auditory perception of higher-order stencils is also a topic that needs further investigation, in order to be able to define more meaningful values for the wave speed error margin ϵ, which relate to accuracy as well as isotropy of the stencil. Moreover, whereas only 'large-star' stencils have been examined in this paper, more general higher-order stencils can lead to even better approximations of the wave equation and less dispersion error, although it is uncertain whether using a more complicated the update equation is worth the investment.

A widely studied and implemented boundary for the second-order wave equation is the Locally Reacting Surfaces method [3], [4], applied to the SRL or IWB, which is capable of providing good results in both simple and complex geometries. An optimal, higher-order scheme will require a new boundary implementation comparable to the LRS, which is not trivial for any reflectivity other than $r = -1$ (i.e. phase-reversing perfect reflection). This problem is subject to further research and testing needs to be solved to enable a wider take-up of higher-order stencils.

ACKNOWLEDGMENT

This work is sponsored in part by a University of York Department of Electronics scholarship and the Huygens Scholarship Programme by the Dutch Ministry of Education. The raw audio files and graphs presented in this paper can be found at [43].

REFERENCES

[1] L. Savioja, T. J. Rinne, and T. Takala, "Simulation of room acoustics with a 3-D finite difference mesh," in *Proc. International Computer Music Conference*, 1994, pp. 463–466.
[2] D. Botteldooren, "Finite-difference time-domain simulation of low-frequency room acoustic problems," *J. Acoustical Society of America*, vol. 98, no. 6, pp. 3302–3308, 1995.
[3] K. Kowalczyk and M. van Walstijn, "Room acoustics simulation using 3-D compact explicit FDTD schemes," *IEEE Trans. Acoustics, Speech, and Language Processing*, vol. 19, no. 1, pp. 34–46, 2011.
[4] C. J. Webb and S. Bilbao, "Computing room acoustics with CUDA - 3D FDTD schemes with boundary losses and viscosity," in *IEEE International Conference on Acoustics, Speech and Signal Processing*, 2011, pp. 317–320.
[5] Odeon. Ray Tracing—Odeon [Online]. Available: http://www.odeon.dk/ray-tracing, Last accessed: July 16, 2013

[6] S. Siltanen, T. Lokki, and L. Savioja, "Rays or waves? Understanding the strengths and weaknesses of computational room acoustics modeling techniques," in *Proc. International Symposium on Room Acoustics 2010*, Aug. 2010, pp. 1–6.
[7] B.-I. Dalenbäck, "Verification of prediction based on randomized tail-corrected cone-tracing and array modeling," in *137th Convention of the Acoustical Society of America*, 1999.
[8] T. Funkhouser, I. Carlbom, G. Elko, G. Pingali, M. Sondhi, and J. West, "A beam tracing approach to acoustic modeling for interactive virtual environments," in *Proc. SIGGRAPH 98*, Jul. 1998, pp. 21–32.
[9] T. Funkhouser, N. Tsingos, I. Carlbom, G. Elko, M. Sondhi, J. E. West, G. Pingali, P. Min, and A. Ngan, "A beam tracing method for interactive architectural acoustics," *J. Acoustical Society of America*, vol. 115, no. 2, pp. 739–756, Feb. 2004.
[10] F. Antonacci, M. Foco, A. Sarti, and S. Tubaro, "Fast tracing of acoustic beams and paths through visibility lookup," *IEEE Trans. Audio, Speech, and Language Processing*, vol. 16, no. 4, pp. 812–824, 2008.
[11] E.-M. Nosal, M. Hodgson, and I. Ashdown, "Improved algorithms and methods for room sound-field prediction by acoustical radiosity in arbitrary polyhedral rooms," *J. Acoustical Society of America*, vol. 116, no. 2, pp. 970–980, 2004.
[12] S. Siltanen, T. Lokki, S. Kiminki, and L. Savioja, "The room acoustic rendering equation," *J. Acoustical Society of America*, vol. 122, no. 3, pp. 1624–1635, 2007.
[13] N. Tsingos, T. Funkhouser, A. Ngan, and I. Carlbom, "Modeling acoustics in virtual environments using the uniform theory of diffraction," in *Proc. ACM SIGGRAPH 2001*, Aug. 2001, pp. 545–552.
[14] S. Siltanen and T. Lokki, "Diffraction modelling in acoustic radiance transfer method," in *Proc. Acoustics'08 Paris*, 2008.
[15] C. Erkut and M. Karjalainen, "Finite difference method vs. digital waveguide method in string instrument modeling and synthesis," in *Proc. International Symposium on Musical Acoustics*, 2002.
[16] J. O. Smith, "On the equivalence of the digital waveguide and finite difference time domain schemes," [Online]. Available: http://arxiv.org/abs/physics/0407032 2004
[17] D. T. Murphy and M. J. Beeson, "The KW-boundary hybrid digital waveguide mesh for room acoustics applications," *IEEE Trans. Audio, Speech, and Language Processing*, vol. 15, no. 2, pp. 552–564, 2007b.
[18] W. Yu, R. Mittra, T. Su, Y. Liu, and X. Yang, *Parallel Finite-Difference Time-Domain Method*. : Artech House, 2006.
[19] R. Mehra, N. Raghuvanshi, L. Savioja, M. C. Lin, and D. Manocha, "An efficient GPU-based time domain solver for the acoustic wave equation," *Applied Acoustics*, vol. 73, pp. 83–94, 2012.
[20] J. J. López, D. Carnicero, N. Ferrando, and J. Escolano, "Parallelization of the finite-difference time-domain method for room acoustics modelling based on CUDA," *Mathematical and Computer Modelling*, vol. 57, pp. 1822–1831, Apr. 2013.
[21] A. P. Southern, D. T. Murphy, T. Lokki, and L. Savioja, "The perceptual effects of dispersion error on room acoustic model auralization," in *Proc. Forum Acusticum 2011*, Aalborg, Denmark, 2011.
[22] N. Raghuvanshi, R. Narain, and M. C. Lin, "Efficient and accurate sound propagation using adaptive rectangular decomposition," *IEEE Trans. Visualization and Computer Graphics*, vol. 15, no. 5, pp. 789–801, 2009.
[23] N. Raghuvanshi, J. Snyder, R. Mehra, M. C. Lin, and N. Govindaraju, "Precomputed wave simulation for real-time sound propagation of dynamic sources in complex scenes," in *Proc. ACM SIGGRAPH 2010*, Jul. 2010, vol. 29, no. 4.
[24] K. Kowalczyk, "Boundary and medium modelling using compact finite difference schemes in simulations of room acoustics for audio and architectural design applications," Ph.D. dissertation, Queen's University Belfast, , Nov. 2008.
[25] G. Fairweather and A. R. Mitchell, "A high accuracy alternating direction method for the wave equation," *IMA J. Applied Mathematics*, vol. 1, no. 4, pp. 309–316, 1965.
[26] N. Borrel-Jensen, "Real-time auralisation of the lower frequency sound field using numerical methods on the gpu," Master's thesis, Rheinisch-Westfälische Technische Hochschule Aachen, , Jun. 2012.
[27] M. Ciment and S. H. Leventhal, "Higher order compact implicit schemes for the wave equation," *Mathematics of Computation*, vol. 29, no. 132, pp. 985–994, 1975.
[28] S. Bilbao and B. Hamilton, "Construction and optimization techniques for high order schemes for the two-dimensional wave equation," in *Proc. International Conference on Acoustics*, 2013.
[29] B. Hamilton and S. Bilbao, "Fourth-order and optimised finite difference schemes for the 2-D wave equation," in *Proc. 16th Conference on Digital Audio Effects (DAFx-13)*, 2013, to be published.
[30] S. Bilbao, "Modeling of complex geometries and boundary conditions in finite difference/finite volume time domain room acoustics simulation," *IEEE Trans. Audio, Speech, and Language Processing*, vol. 21, no. 7, pp. 1524–1533, 2013.
[31] P. Micikevicius, "3D finite difference computation on GPUs using CUDA," in *Proc. Second Workshop on General Purpose Processing on Graphics Processing Units*, 2009, pp. 79–84.
[32] J. C. Strikwerda, *Finite Difference Schemes and Partial Differential Equations*, 2nd Ed. ed. : Society for Industrial and Applied Mathematics, 2004.
[33] R. Courant, K. O. Friedrichs, and H. Lewy, "Über die partiellen Differenzengleichungen der mathematischen Physik," *Mathematische Annalen*, vol. 100, no. 1, pp. 32–74, Dec. 1928.
[34] S. Bilbao, *Numerical Sound Synthesis, Finite Difference Schemes and Simulation in Musical Acoustics*. : John Wiley & Sons, 2009.
[35] B. Fornberg, "Generation of finite difference formulas on arbitrarily spaced grids," *Mathematics of Computation*, vol. 51, no. 184, pp. 699–506, 1988.
[36] J. H. Mathews and K. K. Fink, *Numerical Methods Using Matlab*. : Prentice Hall Inc., 2004, Section 6.2: Numerical Differentiation Formulas.
[37] L. Savioja, "Real-time 3D finite-difference time-domain simulation of low- and mid-frequency room acoustics," in *Proc. 13th International Conference on Digital Audio Effects (DAFx-10)*, 2010.
[38] J. B. Schneider, C. L. Wagner, and O. M. Ramahi, "Implementation of transparent sources in fdtd simulations," *IEEE Trans. Antennas and Propagation*, vol. 46, no. 8, pp. 1159–1168, 1998.
[39] M. Karjalainen and C. Erkut, "Digital waveguides versus finite difference structures: Equivalence and mixed modeling," *J. Applied Signal Processing*, vol. 7, pp. 978–989, 2004.
[40] N. Tsingos, "Using programmable graphics hardware for acoustics and audio rendering," in *Proc. 127th Convention of the Audio Engineering Society*, Oct. 2009.
[41] L. Savioja, V. Välimäki, and J. O. Smith, "Audio signal processing using graphics processing units," *J. Audio Engineering Society*, vol. 59, no. 1/2, pp. 3–19, 2011.
[42] L. Savioja and V. Välimäki, "Interpolated 3-D digital waveguide mesh with frequency warping," in *Proc. IEEE International Conference on Acoustics, Speech, and Signal Processing*, 2001.
[43] J. van Mourik, "Jelle van Mourik—Publications," [Online]. Available: http://www.jellevanmourik.com/publications Last accessed: July 18, 2014

Jelle van Mourik Jelle van Mourik is currently a Ph.D. student at the University of York, Department of Electronics. He also works as an Audio Programmer at Sony Computer Entertainment Europe's London Studio. He received his B.Sc. (Hons) *summa cum laude* at University College Roosevelt in Middelburg in a combined degree of Mathematics, Physics, and Computer Science, with a minor in Musicology. His research interests include virtual acoustic modelling, physical instrument modelling, and computer graphics.

Damian Murphy Damian T. Murphy received the B.Sc. (Hons) degree in mathematics, the M.Sc. degree in music technology, and the D.Phil. degree in music technology, all from the University of York, UK, in 1993, 1995, and 2000, respectively. He is a Reader in the AudioLab based in the Department of Electronics, University of York, where he has worked since 2000 and is a Visiting Lecturer in the Department of Speech, Music, and Hearing, KTH, Sweden and has held visiting researcher positions at a number of universities internationally. His research interests include acoustic modeling and spatial audio. He is a member of the Audio Engineering Society.